



Original Article

# Investigation of the Lamellar Grains of Graft-type Polymer Electrolyte Membranes for Hydrogen Fuel Cell Application using Ultrasmall-angle X-ray Scattering

Lam Hoang Hao<sup>1,2</sup>, Dinh Tran Trong Hieu<sup>1,2,3</sup>, Tran Hoang Long<sup>1,2</sup>,  
Dang Van Hoa<sup>1,2</sup>, Tran Thanh Danh<sup>1,2</sup>, Tran Van Man<sup>1,2</sup>, Le Quang Luan<sup>4</sup>,  
Huynh Truc Phuong<sup>1,2</sup>, Pham Thi Thu Hong<sup>5</sup>, Tran Duy Tap<sup>1,2,\*</sup>

<sup>1</sup>University of Science, 227 Nguyen Van Cu, District 5, Ho Chi Minh City, Vietnam

<sup>2</sup>Vietnam National University, Ho Chi Minh City, Linh Trung, Thu Duc, Ho Chi Minh City, Vietnam

<sup>3</sup>Le Thanh Ton High school, 124, 17 Street, District 7, Ho Chi Minh City, Vietnam

<sup>4</sup>Biotechnology Center of Ho Chi Minh City, 2374 Highway 1, District 12, Ho Chi Minh City, Vietnam

<sup>5</sup>Research and Development Center for Radiation Technology, 202A Street 11, Thu Duc, Ho Chi Minh City, Vietnam

Received 17 April 2021

Revised 10 September 2021; Accepted 11 September 2021

**Abstract:** The extensive ultrasmall-angle X-ray scattering measurements are performed in order to investigate the changes of lamellar grains of poly (styrenesulfonic acid) - grafted poly (ethylene-co-tetrafluoroethylene) polymer electrolyte membranes (ETFE-PEMs) that occur during the alteration of grafting degree (GD) under dry and immersed conditions. The lamellar grains of three series of the samples (polystyrene-grafted ETFE films and dry and hydrated ETFE-PEMs) are formed during the grafting process and develop independently with the change of the lamellar stacks. Interestingly, three series of samples exhibit a very similar trend of lamellar grain at any GD and a significant amount of graft chains is observed directly in the region between the grains ( $GD \leq 59\%$ ) and outside of the grain network structures ( $GD > 59\%$ ). This observation indicates: i) The formation of the lamellar grains; ii) The rapid changes in characteristic sizes of the lamellar grains compared with the lamellar stacks; and iii) The newly generated phases consisting of only the graft materials. These findings explain why the lamellar grains and the graft chains play an important role in the higher proton conductivity and compatible tensile strengths of the membranes, compared with Nafion, at the immersed and severe operating conditions.

**Keywords:** Fuel cells, membranes, polyelectrolytes, lamellar, X-ray.

\* Corresponding author.

E-mail address: [tdtap@hcmus.edu.vn](mailto:tdtap@hcmus.edu.vn)

<https://doi.org/10.25073/2588-1140/vnunst.5216>

## 1. Introduction

Proton exchange membrane (PEM) fuel cells have attracted many interests in solving of the environmental problems due to their advantages over other fuel cells in terms of the clean and efficient power generation and lower operating temperature. They are expected to reduce fossil fuel consumption, which is believed to be the primary source causing climate change [1]. PEM, which consists of super acid groups (i.e., sulfonic acid), has been considered as one of the key components in achieving the high fuel-cell performance because of its unique fuel-cell properties such as ionic conductance, mechanical strength, thermal and chemical stability. When a dry PEM is immersed in water, the hydrophilic chains with sulfonic ion groups can absorb water and form the interconnected ion channels inside the hydrated regions. At the same time, the acid dissociates to release the mobile protons and hence the proton conductivity is created. Macro and microphase separations, viz., crystalline morphologies, conducting layers (ion channels), characteristic domain sizes, and distribution and connection of ionic groups and water in the conducting layers and around the crystalline phases are believed to play an important role in the conductivity and mechanical integrity of the PEMs [2-4]. Currently, the main challenges of improving the conductivity and mechanical strength of the PEMs are the lack of detailed information on the simultaneous changing of the macro and microstructures when the membranes are exposed to the change of the operating conditions such as temperature and humidity. Therefore, in order to improve the performance of the PEM fuel cells, it is highly desirable to have a deeper understanding of their structural changes under the above-mentioned operational conditions. In previous works [5, 6], we have reported the synthesis and characterization of poly(styrenesulfonic acid) (PSSA)-grafted poly(ethylene-co-tetrafluoroethylene) polymer electrolyte membranes (ETFE-PEMs) within a wide range of ion exchange capacity (IEC) at the dry and humid conditions. The obtained results

showed that the ETFE-PEMs have the proton conductivities that are less dependent on the relative humidity (RH) and their mechanical strength and conductivity relate strongly to the PEM crystallinities. The hierarchical structures of the membranes were then investigated using the small-and ultrasmall-angle X-ray scattering (SAXS/USAXS) [7-9]. It was found that, for the ETFE-PEMs with high IECs ( $> 2.7$  mmol/g), a higher conductivity at 30% RH and compatible tensile strength at 100% RH and 80 °C, in comparison with Nafion-212, were originated respectively from the well-interconnected ion channels around the lamellar grains and the remaining lamellar crystals and grains as well. However, within these studies, only the correlation of Bragg-spacing of lamellar grains was reported and it was used to model the hierarchical structures and elucidated the structure-property relationship, whereas the precise parameters of the lamellar grains and the variation of their characteristic structural sizes during the change of grafting degree (GD) under the dry and immersed conditions were not evaluated.

The present study reports the detailed and systematic investigation on the evolution of the lamellar grains and the variation of their characteristic parameters with respect to the ETFE-PEMs as well as the evolution of the precursor original ETFE and styrene-grafted films (grafted-ETFE) using USAXS. As a starting point to understand the structure-property relationship, the higher-order crystalline structures of the membranes as a function of GD were investigated under the dry state and water saturation. On the basis of the results obtained from the small-angle scattering methods, the structure-property interplay was then essentially re-evaluated.

## 2. Experimental

### 2.1. Materials and Sample Preparation

Details on the materials and sample preparations were described in our previous studies [5, 6]. Briefly, the pristine ETFE films

with a thickness of 50  $\mu\text{m}$  were preirradiated by  $^{60}\text{Co}$   $\gamma$ -rays with an absorbed dose of 15 kGy and then immersed in a styrene solution at 60  $^{\circ}\text{C}$  for the grafting polymerization to obtain the polystyrene grafted ETFE (grafted-ETFE). The GD of the grafted-ETFE is determined by using the following equation:

$\text{GD} (\%) = (W_g - W_0/W_0) \times 100$ , where  $W_0$  and  $W_g$  are the weights of the films before and after the graft polymerization, respectively. Note that the polystyrene-grafted ETFE films were subsequently immersed in a toluene solution at 50  $^{\circ}\text{C}$  for 24 h to remove the homo-polymers and the residual monomers before the GD calculation. The grafted-ETFE was then immersed in 0.2 M chlorosulfonic acid in 1,2-dichloroethane at 50  $^{\circ}\text{C}$  for 6 h. The membrane was washed with pure water at 50  $^{\circ}\text{C}$  for 24 h to obtain an ETFE-PEM. The detailed characterization methods were represented in the previous works [5, 6].

## 2.2. FE-SEM Measurement

The surface morphology was observed by using a field-emission scanning electron microscope (FE-SEM) manufactured by Hitachi Company (S-4800) without an additional surface treatment or coating of the samples. The images were obtained using a secondary electron imaging mode of FE-SEM with an accelerating voltage of 1 kV and a working distance of 3.5 mm. The secondary electron signals were collected from both in-lens and side detector.

## 2.3. SAXS Measurement

The equipment and detailed procedures for the SAXS measurements were described in our previous work [7-9]. Briefly, the SAXS measurement was performed using two in-house SAXS spectrometers (NIMS-SAXS-II and NIMS-SAXS-III) at the National Institute of Material Science (NIMS) and USAXS at Super Photon ring-8 GeV (SPring-8), Japan. At NIMS, fine-focus SAXS instruments with X-rays of Mo- $K_{\alpha}$  ( $\lambda_{\alpha} = 0.07$  nm) (Rigaku NANO-Viewer, Tokyo, Japan) and Cr- $K_{\alpha}$  ( $\lambda_{\alpha} = 0.23$  nm) (Bruker NanoSTAR, Germany) were utilized. The sample-detector distances in

the Mo-SAXS and Cr-SAXS were set at 35.0 and 105.6 cm, respectively. At SPring-8, the SAXS measurements were performed by USAXS at the beamline BL19B2 using an incident X-ray energy of 18 keV ( $\lambda = 0.0688$  nm). The sample-detector distance was 42 m. Thus, both the pinhole SAXS measurements at NIMS and SPring-8 were carried out to cover a wide  $q$ -range ( $q = 0.004$ - $3.13$  nm $^{-1}$ ), which corresponds to the Bragg-spacing of 2-1570 nm. Here,  $q$  is referred to as the modulus of the scattering vector, which equals to  $4\pi\sin\theta/\lambda$ , where  $2\theta$  is the scattering angle and  $\lambda$  is the wavelength of the incident X-rays.

## 2.4. SAXS Analysis

To determine the characteristic sizes of lamellar grains, the USAXS profiles were analyzed based on one-dimensional correlation function,  $\gamma_{1D}(r)$  [10, 11]. Using the scattering intensity,  $I(q)$ , the one-dimensional correlation function can be obtained as [10, 11]:

$$\gamma_{1D}(r) = \frac{1}{\gamma(0)} \int_0^{\infty} I(q) q^2 \cos(qr) dq \quad (1)$$

where  $r$  is the direction along which the electron density is measured, and  $\gamma(0)$  is the scattering invariant, which is often defined based on the invariant  $Q_1$  of the form as:

$$Q_1 = \int_0^{\infty} I(q) q^2 dq \quad (2)$$

Since the experimentally accessible  $q$  range is finite, the extrapolation to both low and high  $q$  regions is necessary for the integration in Equations (1) and (2). Within the present work, the extrapolation to zero  $q$  was performed by using the Debye-Bueche model [12, 13]:

$$I(q) = \frac{A}{(1+a_c^2 q^2)^2} \quad (3)$$

where  $A$  is constant and  $a_c$  is a correlation length, whose values can be determined from the plot  $I(q)^{-1/2}$  versus  $q^2$  at the low- $q$  region. The extrapolation to large- $q$  region was carried out by employing the Porod model, whose equation is written as [14-17]:

$$I(q) = \frac{k_p \exp(-\sigma^2 q^2)}{q^4} \quad (4)$$

where  $\sigma$  is a parameter related to the thickness of the interface between the two phases. As the

present work employed the simplified two-phase model, the values of  $\sigma$  in Equation (4) should be equal to zero, indicating that there is no interference between the two above-mentioned phases.  $k_p$  was obtained by curve fitting the intensity profile at large- $q$  region.

### 3. Results and Discussion

The chemical structures and polymeric compositions of the same precursor grafted films and ETFE-PEMs have been previously examined by using the FT-IR measurements [6]. Based on these characterizations, the styrene was confirmed to be grafted onto the ETFE film and the grafted film was sulfonated by introduction of the  $-\text{SO}_3\text{H}$  group. Figure 1 presents the Lorentz-corrected SAXS profiles of the original SAXS data [7-9]. This figure shows that the shoulder-like peaks to be pronounced. The pronounced peaks seen in the low- $q$  region ( $q < 1.5 \times 10^{-1} \text{ nm}^{-1}$ ) are observed even at high GD values (GD  $\geq 59\%$ ), which indicate the strong development of the grain structures (lamellar grains) with the increase of GD. The new shoulder-like peak observed in the very low- $q$  region ( $q < 1.5 \times 10^{-1} \text{ nm}^{-1}$ ) implies the presence of the lamellar grains at a scale higher than that seen in the lamellar stacks [7-9]. At the localized scale, the peak corresponds probably to the average correlation distance between the two grains, which are composed of the crystalline regions and graft chains incorporated in the amorphous ETFE regions [7, 18]. Connection between the two grains is a newly generated phase consisting of the graft chains only. Thus, it is generally assumed that the above phase presents a new two-phase structure, which also has a layered configuration (lamellar grain), at least at a localized scale. Thus, we also utilize the one-dimensional correlation function in order to determine the characteristic parameters of the lamellar grains using the same procedures as employed for the lamellar stacks [7, 8]. Since the ETFE films are one-dimensionally oriented due to the extrusion drawing step in the film preparation, the one-dimensional correlation

function,  $\gamma_{1D}(r)$ , were calculated by Equation (1) (see Experimental) using the SAXS data with the extrapolation to both low- and high- $q$  regions and listed in Figure 2. The lamellar period ( $L_{1D} = 192 \text{ nm}$ ) and crystalline lamellar thickness ( $L_c = 41 \text{ nm}$ ) can be determined from the positions of the first maximum and the crossing point between the baseline and the sloping line of the self-correlation triangle in the plot of  $\gamma_{1D}(r)$  (Figure 2), respectively [10]. Thus,  $L_a = 151 \text{ nm}$  can be easily obtained.

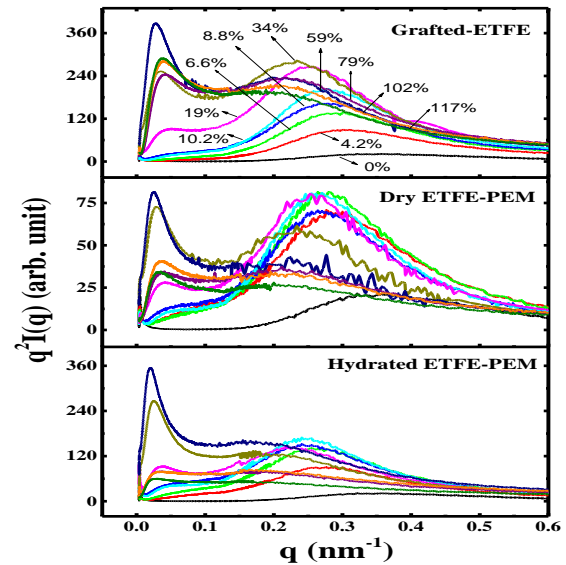


Figure 1. Lorentz-corrected SAXS profiles in the linear-linear plots of the original SAXS profiles of the grafted-ETFE films and the corresponding dry and hydrated ETFE-PEMs with GD = 0-117%.

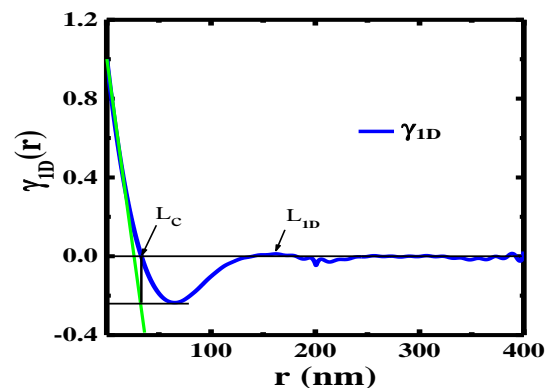


Figure 2. The one-dimensional correlation function of the lamellar grains is calculated from the SAXS data of grafted-ETFE with GD = 19% [7, 8].

Figures 3a-3c show the  $\gamma_{1D}(r)$  plots of the lamellar grains obtained for the grafted-ETFE films and the corresponding dry and hydrated ETFE-PEMs with GD = 0-117%. It is worth mentioning here that to determine this  $\gamma_{1D}(r)$  function, the extrapolation of  $I(q)$  to zero- $q$  (the Debye-Bueche model) and high- $q$  regions (the Porod model) was performed in the present work. Similar to the lamellar stacks [7, 8], there are small differences between the values of  $\gamma_{1D}(r)$  function obtained for the grafted-ETFE films and dry ETFE-PEMs (Figures 3a and 3b) and those obtained for the hydrated ETFE-PEMs (Figure 3c), indicating a similarity in the organization of the lamellar grains in the three series of samples. Very different from the behavior of  $\gamma_{1D}(r)$  function obtained for the lamellar stacks, the oscillation in the values of  $\gamma_{1D}(r)$  function obtained for the lamellar grains is still pronounced even at high GD values (GD  $\geq$  59%), which is in good agreement with the features of the original SAXS profiles (Figure 1) [7, 8]. This behavior indicates the strong development of lamellar grains with the increase of GDs.

Figures 4a-4c present the values of  $L$ ,  $L_a$ , and  $L_c$  obtained within the three series of samples as functions of GD. By increasing GD from 4.2 to 59%, the  $L$  values of the grafted-ETFE films increase from 96 to 249 nm, whereas they increase from 109 to 267 nm and from 111 to 279 nm within the dry and hydrated membranes, respectively. The  $L$  values of the lamellar grains increase by a factor of 2.5 when GD increases from 4.2 to 59%. This increase is much higher than that obtained within the lamellar stacks [7, 8], which increases by a factor of 1.3 only. In addition, the crystal size of lamellar stacks did not change, whereas the crystal size  $L_c$  of the lamellar grains increases from 22 to 47 nm in the grafted-ETFE films and from 24 to 53 nm in the dry and hydrated membranes (Figure 4c). The increase of  $L$  in the grafted-ETFE films relates partially to the expansion of  $L_a$  caused by the grafting effects as shown in Figure 4b, similar as the case of lamellar stacks [7, 8]. However, this increase of  $L$  is also caused by the normal

increase of  $L_c$  and possible rearrangement of the layered grain structures outside of the lamellar stacks (i.e., between the grains). Similar changes of  $L$ ,  $L_c$ , and  $L_a$  are also observed in the dry and hydrated membranes. Also, in comparison with the grafted-ETFE films, the sulfonation process (dry ETFE-PEM) and immersed condition (hydrated ETFE-PEM) cause a further increase of  $L$  with the average percentage of 14.8 and 21.1%, respectively. This increase of  $L$  is much higher than that of the lamellar stacks (increasing only 6.9 and 11.9%, respectively).

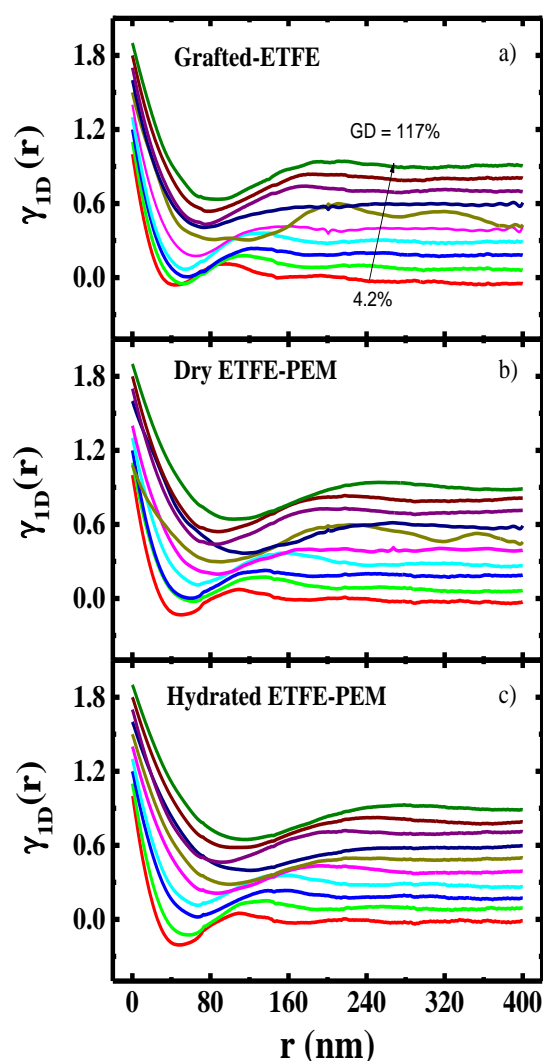


Figure 3. One-dimensional correlation functions of the lamellar grains obtained within (a) the grafted-ETFE films and the corresponding (b) dry and (c) hydrated ETFE-PEMs with GD = 0-117%.

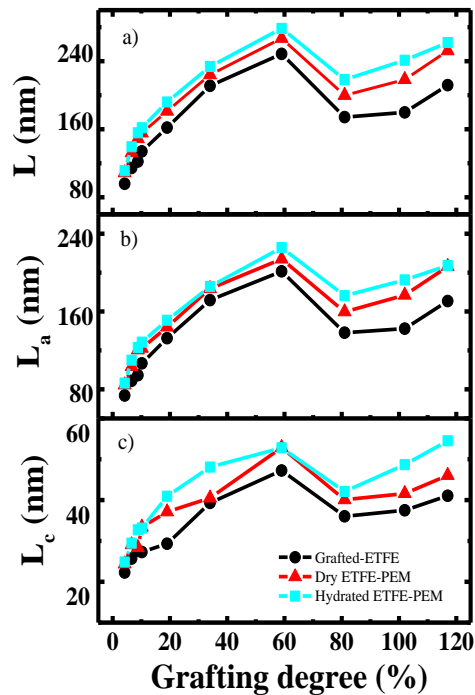


Figure 4. (a) Plots of the lamellar period ( $L$ ), (b) amorphous lamellar thickness ( $L_a$ ), and (c) crystalline lamellar thickness ( $L_c$ ) as functions of GD of the grafted-ETFE films and the corresponding dry and hydrated ETFE-PEMs with GD = 0-117%.

The values of  $L$  obtained within the grafted-ETFE films suddenly decrease from 249 to 174 nm with increasing GD from 59 to 79% and then slightly increase from 174 to 211 nm when GD increases from 79 to 117%. Similar behavior is also observed for  $L_a$  and  $L_c$  in the same GD range (Figures 4b and 4c). The discontinuous changes in  $L$ ,  $L_a$ , and  $L_c$  of the grafted-ETFE in the GD region of 59-79% strongly indicate that a phase transition from the oriented grains to the grain network structures in the grafted-ETFE morphology induced by the introduction of the PS grafts has occurred. This phase transition has been discussed in our previous publications [7, 8]. Moreover, this behavior also illustrates clearly that the amorphous PS grafts have been excluded from the intergrain regions but not the interlamellar ones, resulting in a newly generated phase, which consists of only PS grafts located outside

of the grain network structures. As a result, a new layered structure is formed at a scale larger than that presented in the lamellar grains [7, 8]. In fact, this new layered structure consists of (1) a newly generated phase consisting of the graft chains only and (2) a grain network structure as illustrated in Figure 7. Similar results are also obtained for the dry and hydrated membranes. It is worthwhile noticing that before and after the phase transition, the characteristic parameters of  $L_a$  and  $L_c$  obtained within the lamellar grains are still remained. However, this feature was not considered in the previously proposed model of the lamellar grains [7, 18]. Thus, within the present work, the model for the lamellar grains and the grain network structures has been revised as illustrated in Figure 7.

It is worth noting that the values of  $L$  obtained from the  $\gamma_{1D}(r)$  plots for the lamellar grains agree well with those determined from the Lorentz-corrected SAXS profiles reported in the previous works (Figure 5) [7]. Consequently, the determination of the lamellar periods based simply on the Bragg's law in the SAXS profiles could lead sometime to inaccurate results in the weak ordering systems [11]. In other words, the  $L_L$  values, which are estimated from the peak maxima in the Lorentz-corrected SAXS profiles, should be overestimated in the previous report [7]. Accordingly, together with taking into account the results from our previous investigations [5-9], we will take in advantage of the one-dimensional correlation function for detailed analysis of the SAXS data for the predictions of the lamellar two-phase system.

Figure 6a shows the surface LVSEM image at a magnification of 50 K for the original ETFE. Besides providing topographic information essentially, secondary electron image (SEI) also gives some features on compositional contrast at the surface since few back-scattered electrons are collected by the secondary electron detector.

As can see in Figure 6a, the low-oriented bright fibers and dark substrate relate to the ETFE crystalline phase with higher electron density and

ETFE amorphous phase with lower electron density, respectively. Shown in Figure 6b is the LVSEM image of ETFE-PEM at GD of 19%.

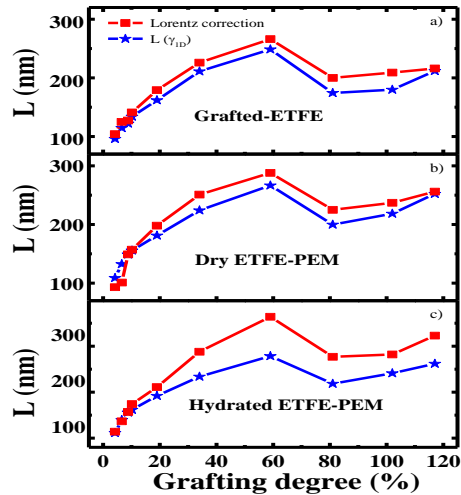


Figure 5. Average lamellar periods of the lamellar grains obtained within different evaluation methods, namely the position of maxima  $q^*$  of the Lorentz-corrected SAXS profiles using the Bragg's law of the one-dimensional correlation function  $\gamma_D(r)$ .

This image reveals the arrangement of visible lamellar grains. For the ETFE-PEM, the charging problem can be minimized when an accelerating voltage of 1 kV is applied. The reason is that this low accelerating voltage results in a low penetration depth of the primary electron beam in the ETFE-PEM but at the same time it yields the high secondary electrons. Thus, the presented LVSEM image shows the surface topography of the ETFE-PEM. The image also presents the aligned repeat of lamellae with diameters and lengths ranging from 20 to 50 nm and from 150 to 250 nm, respectively. Consequently, the LVSEM image is a discernible evidence for the differences between the lamellar grains. This result is comparable with that obtained within the SAXS measurement described above. Note that the features of the lamellar gains with the aligned bright stripes of 200-300 nm were also observed using the cross-section FE-SEM images [7]. Thus, the oriented crystallite domains consisting of the lamellar grains are observed in the bulk and also at the surface of ETFE-PEMs.

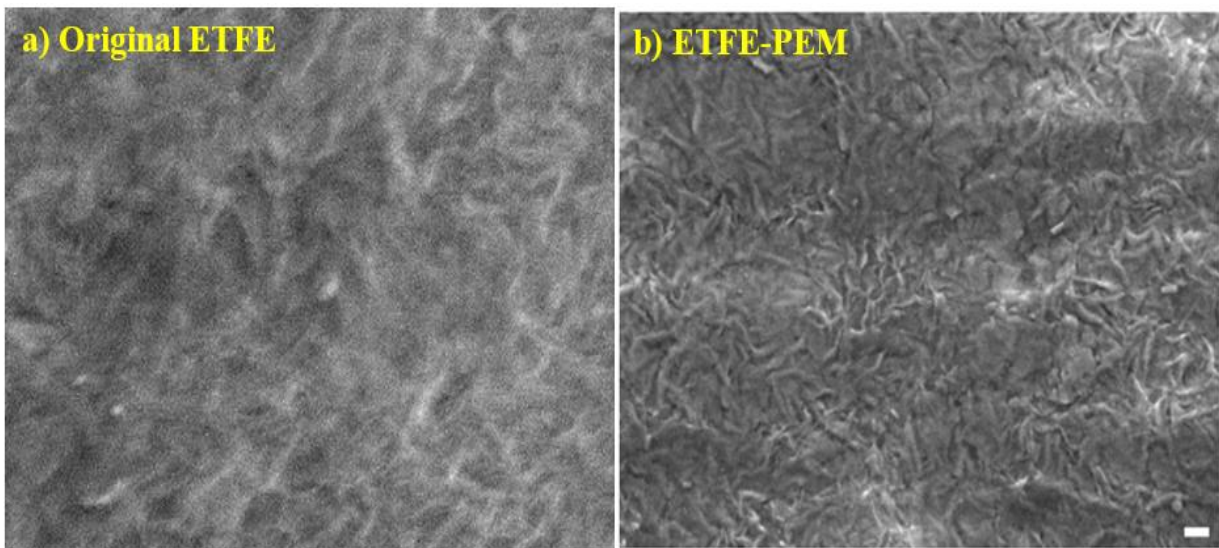


Figure 6. a) Low voltage scanning electron microscopic (LVSEM) images of the original ETFE and b) ETFE-PEM at a GD of 19% (magnification = 50,000 $\times$ , scale bar = 100 nm).

Figure 7 shows a schematic illustration of the morphology change in the higher-order structures of three series of samples with GDs of

4.2-117%. The lamellar grains are formed at the very early stage of the grafting (GD = 4.2%) and then developed significantly with increasing

GD. At the same time, the graft chains are introduced into the lamellar grains in the GD region of 0-59%. They are then introduced only into the lamellar grain network structures when GD is higher than 59%. Moreover, in the GD region of 0-59%, the graft chains introduced into the lamellar grains are much higher than those developed in the lamellar stacks [7, 8]. It is worth

mentioning that structures of the lamellar stacks and lamellar grains are still remained even at high GD values ( $GD > 59\%$ ). For the first time, the detailed characteristic sizes of the lamellar grains and their phase separation in the graft-type PEMs through the preparation procedures at different values of GD are elucidated clearly.

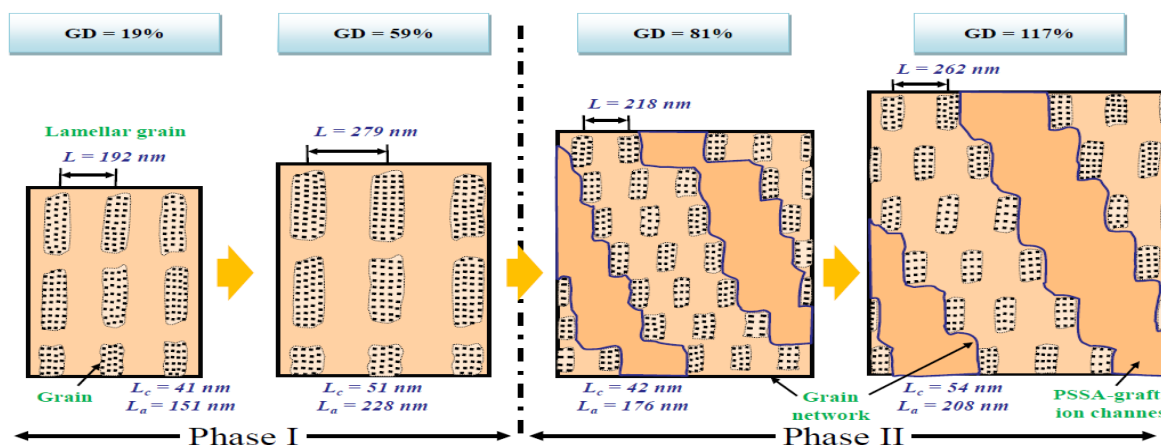


Figure 7. Schematic illustrations of the morphology change of lamellar grains of the grafted-ETFE films and dry and hydrated ETFE-PEMs at GDs of 4.2-117%.

#### 4. Conclusion

The present investigation shows clearly the change of the characteristic parameters obtained for the lamellar grains of the graft-type PEMs with changing the values of GD under the dry and immersed conditions using the USAXS. The results obtained indicate that the sulfonation process and immersed conditions do not alter the organization of the lamellar grains in the grafted-ETFE films at any values of GD. Thus, the styrene-grafted ETFE films and dry and hydrated ETFE-PEMs exhibit very similar lamellar grains. The lamellar grains are formed only during the grafting process and developed independently with the change of the lamellar stacks. The significant amount of the graft chains is observed directly outside of the grain network structures ( $GD > 59\%$ ). This behavior corresponds to: i) The formation of new lamellar grains; ii) The rapid changes in the characteristic sizes of the lamellar grains in comparison with the lamellar stacks; and iii) A newly generated

phase consisting of only the graft materials located between the grains and outside of the grain network structures. The above findings may therefore provide new perspectives toward the optimized unique structures, for example, controllability of the hierarchical structures of the membranes by applying only the grafting process or by changing the crystallinity of the pristine film.

#### Acknowledgements

This research is funded by Vietnam National Foundation of Science and Technology Development (NAFOSTED) under grant number 103.99-2020.59. We also thank Dr. Masota Ohnuma, Dr. Yojiro Oba, Dr. Yasunari Maekawa, Dr. Shin-ichi Sawada, Dr. Shin Hasegawa for their help with the SAXS experiments.

#### References

- [1] B. Smitha, S. Sridhar, A. A. Khan, Solid Polymer Electrolyte Membranes for Fuel Cell Applications a Review, *J. Membr. Sci.*, Vol. 259, 2005, pp. 10-26, <https://doi.org/10.1016/j.memsci.2005.01.035>.

- [2] Y. Liu, J. L. Horan, G. J. Schlichting, B. R. Carire, M. W. Liberatore, S. J. Hamrock, G. M. Haugen, M. A. Yandrasits, S. Seifert, A. M. Herring, A Small-angle X-ray Scattering Study of the Development of Morphology in Films Formed from the 3M Perfluorinated Sulfonic Acid Ionomer, *Macromolecules*, Vol. 45, 2012, pp. 7495-7503, <https://doi.org/10.1021/ma300926e>.
- [3] X. C. Chen, D. T. Wong, S. Yakovlev, K. M. Beers, K. H. Downing, N. P. Balsara, Effect of Morphology of Nanoscale Hydrated Channels on Proton Conductivity in Block Copolymer Electrolyte Membranes, *Nano Lett*, Vol. 14, 2014, pp. 4058-4064, <https://doi.org/10.1021/nl501537p>.
- [4] Q. Berrod, S. Lyonard, A. Guillermo, J. Ollivier, B. Frick, A. Manseri, B. Améduri, G. Gébel, Nanostructure and Transport Properties of Proton Conducting Self-assembled Perfluorinated Surfactants: A Bottom-up Approach Toward PFSA Fuel Cell Membranes, *Macromolecules*, Vol. 48, 2015, pp. 6166-6176, <https://doi.org/10.1021/acs.macromol.5b00770>.
- [5] T. D. Tap, S. Sawada, S. Hasegawa, Y. Katsumura, Y. Maekawa, Poly(ethylene-co-tetrafluoroethylene) (ETFE)-Based Graft-type Polymer Electrolyte Membranes with Different Ion Exchange Capacities: Relative Humidity Dependence for Fuel Cell Applications, *J. Membr. Sci*, Vol. 447, 2013, pp. 19-25, <https://doi.org/10.1016/j.memsci.2013.07.041>.
- [6] T. D. Tap, D. D. Khiem, L. L. Nguyen, N. Q. Hien, L. Q. Luan, P. B. Thang, S. Sawada, S. Hasegawa, Y. Maekawa, Humidity and Temperature Effects on Mechanical Properties and Conductivity of Graft-type Polymer Electrolyte Membrane, *Radiat. Phys. Chem*, Vol. 51, 2018, pp. 186-191, <https://doi.org/10.1016/j.radphyschem.2018.06.033>.
- [7] T. D. Tap, S. Sawada, S. Hasegawa, K. Yoshimura, Y. Oba, M. Ohnuma, Y. Katsumura, Y. Maekawa, Hierarchical Structure-property Relationships in Graft-type Fluorinated Polymer Electrolyte Membranes Using Small - and Ultrasmall-angle X-ray Scattering Analysis, *Macromolecules*, Vol. 47, 2014, pp. 2373-2383, <https://doi.org/10.1021/ma500111x>.
- [8] T. D. Tap, L. L. Nguyen, Y. Zhao, S. Hasegawa, S. I. Sawada, N.Q. Hung, Y. Maekawa, SAXS Investigation on Morphological Change in Lamellar Structures During Propagation Steps of Graft-type Polymer Electrolyte Membranes for Fuel Cell Applications, *Macromol. Chem. Phys*, Vol. 221, 2020, pp. 1900325, <https://doi.org/10.1002/macp.201900325>.
- [9] T. D. Tap, L. L. Nguyen, S. Hasegawa, S. I. Sawada, L. Q. Luan, Y. Maekawa, Internal and Interfacial Structure Analysis of Graft-type Fluorinated Polymer Electrolyte Membranes by Small-angle X-ray Scattering in the High-q Range, *J. Appl. Polym. Sci*, Vol. 137, 2020, pp. 49029, <https://doi.org/10.1002/app.49029>.
- [10] G. R. Strobl, M. Schneider, Direct Evaluation of the Electron Density Correlation Function of Partially Crystalline Polymers, *J. Polym. Sci., Polym. Phys. Ed*, Vol. 18, 1980, pp. 1343-1359, <https://doi.org/10.1002/pol.1980.180180614>.
- [11] C. S. Cruz, N. Stribeck, H. G. Zachmann, F. J. B. Calleja, Novel Aspects in the Structure of Poly (Ethylene Terephthalate) as Revealed by Means of Small Angle X-ray Scattering, *Macromolecules*, Vol. 24, 1991, pp. 5980-5990, <https://doi.org/10.1021/ma00022a013>.
- [12] P. Debye, A. M. Bueche, Scattering by an Inhomogeneous Solid, *J. Appl. Phys*, Vol. 20, 1949, pp. 518-525, <https://doi.org/10.1063/1.1698419>.
- [13] P. Debye, H. R. Anderson, J. H. Brumberger, Scattering by an Inhomogeneous Solid, II, The Correlation Function and Its Application, *J. Appl. Phys*, Vol. 28, 1957, pp. 679-683, <https://doi.org/10.1063/1.1722830>.
- [14] G. Porod, Die Röntgenkleinwinkelstreuung von Dichtgepackten Kolloiden Systemen, *Kolloid-Zeitschrift*, Vol. 124, 1951, pp. 83-114, <https://doi.org/10.1007/BF01512792>.
- [15] G. Porod, Die Röntgenkleinwinkelstreuung von Dichtgepackten Kolloiden Systemen, *Kolloid-zeitschrift*, Vol. 125, 1952, pp. 51-57, <https://doi.org/10.1007/BF01519615>.
- [16] G. Porod, Die Röntgenkleinwinkelstreuung von Dichtgepackten Kolloiden Systemen, II, Teil, *Kolloid-zeitschrift*, Vol. 125, 1952, pp. 108-122, <https://doi.org/10.1007/BF01526289>.
- [17] C. G. Vonk, Investigation of Non-ideal Two-phase Polymer Structures by Small-angle X-ray Scattering, *J. Appl. Crystallogr*, Vol. 6, 1973, pp. 81-86, <https://doi.org/10.1107/S0021889873008204>.
- [18] Y. Zhao, K. Yoshimura, H. Shishitani, S. Yamaguchi, H. Tanaka, S. Koizumi, N. Szekely, A. Radulescu, D. Richter, Y. Maekawa, Imidazolium-based Anion Exchange Membranes for Alkaline Anion Fuel Cells: Elucidation of the Morphology and the Interplay Between the Morphology and Properties, *Soft Matter*, Vol. 12, 2016, pp. 1567-1578, <https://doi.org/10.1039/C5SM02724A>.